CIVIL ENGINEERING

Computational implementation of alternative method for determining the loss of prestressing by deformation of the anchorage in post-tensioning

Iuri Fazolin Fraga[1]* , **Artur Lenz Sartorti[2], Fernando Júnior Resende Mascarenhas[3], João Paulo Boff Almeida[4], Matheus Henrique Morato de Moraes[1] and André Luis Christoforo[1]**

[1]Departamento de Engenharia Civil, Universidade Federal de São Carlos, Washington Luís Highway, s/n, 13565-905, São Carlos, São Paulo, Brazil. [2]Departamento de Engenharia Civil, Centro Universitário Adventista de São Paulo, Engenheiro Coelho, São Paulo, Brazil. [3]Departamento de Engenharia Civil, Universidade de Coimbra, Coimbra, Portugal. [4]Departamento de Engenharia Civil, Instituto Federal de Educação, Ciência e Tecnologia do Ceará, Quixadá, Ceará, Brazil. *Author for correspondence. E-mail: iurifraga@outlook.com

ABSTRACT. Due to its advantages, Prestressed Concrete has been used as a structural element in many buildings worldwide. In order to overcome large spans, limiting the formation of cracks, its application can be visualized, for example, in bridges, viaducts, and building slabs. These structures are executed by stretching steel cables with a subsequent release, introducing compressive stresses in the concrete. However, during this process, stress losses occur in the active reinforcement, requiring forecast by the designers. Quantifying these losses in certain cases is a long and iterative process. The present work aimed to present the computational implementation of an alternative method for determining the loss due to deformation of the anchorage in post-traction. In order to prove its effectiveness, this method was contrasted with two conventional methodologies established in the literature. To this end, two models of beams of the same cross-section were simulated, however, with different spans and cable paths. Both proposed simulations aimed to cover all possible situations for the development of prestressing stress along with the tensioned cables. The alternative method showed minor differences in all measurements compared to the conventional methods, proving its effectiveness. Furthermore, the computational tool, entitled vProt, proved to be reliable in the two proposed simulations, allowing its use in the elaboration and verification of structural projects.

Keywords: prestressed concrete; prestressing loss; post-tensioning; anchorage deformation.

Introduction

To meet the growing demand for construction works such as bridges and buildings, Prestressed Concrete emerged as an evolution of Reinforced Concrete. It aims to mitigate the effects of the low tensile strength of concrete. Its basic premise is the application of previous compression stresses in the region of the cross-section of the element that presents tensile stresses due to the other actions. Thus, when external loading is applied, the final tensile stresses are mitigated by the compressive stresses pre-applied to the element. igure 1 exemplifies this premise presented.
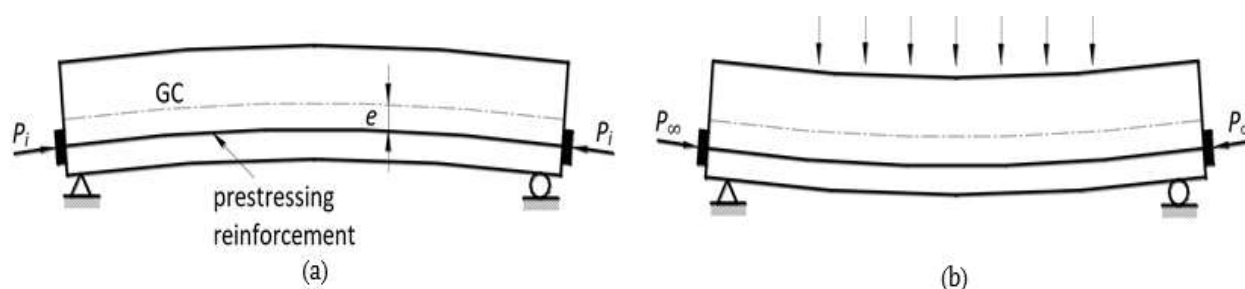

igure 1. Simply supported beam in prestressed concrete: Previous compressive stresses (a) External loading applied (b). Source: Adapted from Bastos (2019a).

Due to its efficiency, many design engineers opt for Prestressed Concrete as a structural alternative to overcome large spans, limiting the formation of cracks in the structural elements. Therefore, prestressing systems are commonly used in bridges, viaducts, and building slabs (Yang, Gong, & Yang, 2020; Ye, Butler, Elshafie, & Middleton, 2020; Michelini, Bernardi, Cerioni, & Belletti, 2020; Araújo, Sales, Silva, Antunes, & Ferreira, 2020).

In Prestressed Concrete, the previous compressive stresses are introduced in the element through the stretching of the steel (active reinforcement) that runs through the entire longitudinal section of the element. When released from the prestressing jack, the steel tends to return to its original position. However, it is prevented by anchorage at the end of the element. This process introduces an initial compressive stress (P_i) in the element (igure 1a) that is directly related to the elongation that occurred in the active reinforcement.

However, during the stretching process and subsequent release of the cables, variables such as the friction between the strand and the sheath; slipping of the anchor wedge; steel relaxation; concrete shortening; among other factors, they produce a series of effects that lead to a decrease in the force P_i. The different reductions of this force characterize the prestressing losses. The designer's responsibility is to estimate them so that in any section, combination of loads or moment in the structure's useful life, both the conditions of use and those of ultimate limit states are satisfied (Carvalho, 2012).

The study of prestressing losses is essential in the elaboration of structural projects, so it is a recurrent topic in the literature, contemplating several studies that explore not only the types and methodologies of quantification but also the application of its algorithms in the determination of other variables involving the prestressing of concrete elements (Caro, Martí-Vargas, & Serna, 2013; Myers & Bloch, 2013; Singh, Yazdani, & Ramirez, 2013; Shao, Pan, Zhao, & Shao, 2014; Asamoto, Kato, & Maki, 2014; Cao, Tao, & Ma, 2015; Ward, Dang, Floyd, & Hale, 2016; Biswal & Ramaswamy, 2017; Guo, Chen, Lu, & Yao, 2017; Křístek & Kadlec, 2017; Breccolotti, 2018; Páez & Sensale, 2018; Abdel-Jaber & Glisic, 2018; Xie, Cui, Yan, & Yu, 2019; Yang, Gong, & Yang, 2020; Ye, Butler, Elshafie, & Middleton, 2020; Breccolotti, 2020).

Based on all the stress losses acting on a prestressed concrete element, the one that will be highlighted in this work is the one arising from the slipping of the anchor wedge after the release of the tensioned cables. Its quantification depends on the type of process used to fabricate the structural element.

There are two prestressing processes applied to a concrete piece: pre-tensioning and post-tensioning. In general, in the pre-tensioning process, the strands are tensioned before concreting the element. In the post-tensioning process, the opposite occurs, i.e., the concrete element is manufactured before the steel cables are stretched. For this, ducts (sheaths) are located along the longitudinal section, and posteriorly they are filled by the strands.

In both processes, when the active reinforcement is released, it recedes a few millimeters towards "inside" the concrete element. With this movement, the anchor wedge is dragged into the conical hole of the wedge holder piece until its crimping is complete. This small setback causes a drop ($\Delta\sigma_p$) in the tensile stress (σ_p) of the previously stretched cables, characterizing the so-called loss due to deformation or slippage of the anchor.

In the pre-tensioning process, there is no friction at the moment of regression of the cables, so its deformation (ε) is assumed to be constant along the longitudinal section. Therefore, the stress reduction ($\Delta\sigma_p$) due to slipping of the anchorage can be estimated through the Law of Hooke, the result of the product of the deformation of the anchorage (ε) times the modulus of elasticity of the prestressing steel (E_p) (Carvalho, 2012).

In post-tensioning process, due to the friction between the cable-sheath assembly, the stress reduction ($\Delta\sigma_p$) decreases until it reaches zero, at the so-called "unmovable" point to the anchorage. Determining the position of this undisplaceable point and the values of $\Delta\sigma_p$ in each analysis section make the quantification process much more laborious than in the case of pre-tensioning.

Conventional methodologies for obtaining the loss by accommodation of the anchorage in post-tensioning are based on iterative processes based on trial and error or approximate estimates (Naaman, 2012; Carvalho, 2012; Cholfe & Bonilha, 2018; Dolan & Hamilton, 2019). However, Marconato & Sartorti (2015) developed a method in which it is possible to determine the stress variation ($\Delta\sigma_p$) in each analysis section through simplified equations. Thus, manual calculation and computational algorithms can be implemented alternatively in the structural development routines of structural projects. The advantage of this method over others is precisely to eliminate initial estimates or guesses, and to organize the problem in the form of a spreadsheet with direct equations. Therefore, it allows for analyzing the number of required sections without hindering implementation.

Based on what has been presented, the main objective of this study is to present the alternative methodology and its efficiency through comparisons with conventional methodologies. The specific objectives are as follows: to synthesize the conventional methodologies for determining the loss due to post-tensioning anchorage deformation proposed by Naaman (2012), Carvalho (2012), Dolan & Hamilton (2019); to present the alternative method proposed by Marconato & Sartorti (2015) implemented in a computational tool; to evaluate the reliability of the alternative methodology based on the simulation of two beams with different spans and cable paths.

Material and methods

For the prestressing loss due to anchorage deformation to be realistically quantified, it is vital to know the loss that precede the moment of anchorage. The different reductions in prestressing effort are classified by item 9.6.3.1 of ABNT NBR 6118 (2014) according to their moment (instant) of occurrence. In post-tensioning, the two recurring types are the immediate losses and the deferred losses over time. The immediate losses occur during the transfer of prestressing to the concrete, while the deferred losses occur progressively over time (ABNT NBR 6118, 2014). Figure 2 illustrates the chronology of quantification of these losses in post-tensioned elements.
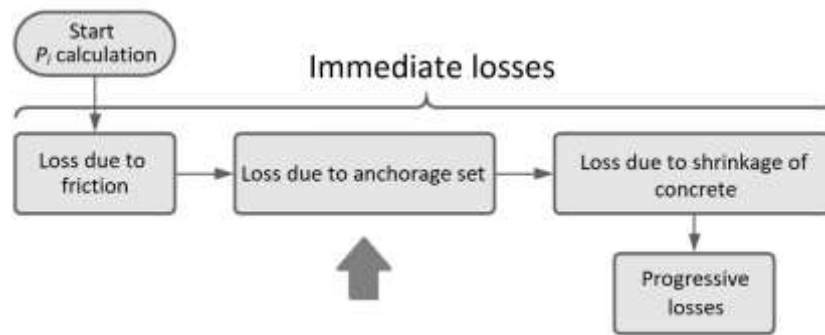

Figure 2. Flowchart of the instant of occurrence of the prestressing losses in post-tensioning.

From Figure 2, the only loss that precedes the moment of anchoring is that arising from the friction between the strand and the sheath. In post-tensioned elements, the ducts (sheaths) almost always have a curved development path and involuntary sinuosities, generating friction during the stretching process. The stress $[\sigma_p(x)]$ after the friction loss in each section of the active reinforcement is given by Equation 1, adapted from ABNT NBR 6118 (2014).

$$\sigma_p(x) = \sigma_{p,i} \cdot e^{-\lambda \cdot x}, \text{ and } \lambda = \mu \cdot \frac{\sum \alpha}{x} + k \tag{1}$$

Where, $\sigma_{p,i}$: Stress in active reinforcement immediately after prestressing is applied; μ: Apparent friction coefficient between the cable and the sheath; $\sum \alpha$: Sum of the deviation angles between the anchor and the x-abscissa point; k: Coefficient of loss per meter caused by unintentional bending of the cable. In the absence of experimental data, k is assumed to be equal to 1% of μ; x: Abscissa of the point where the variation $\Delta\sigma_p(x)$ is calculated, and it is calculated from the anchorage.

As previously mentioned, the anchor slip loss comes from the slight recoil of the prestressed cables, causing a reduction $(\Delta\sigma_p)$ of the acting tensile stress $(\sigma_{p,i})$. Figure 3 illustrates the stress development long the cable during the anchoring process.

In situation A (Figure 3a), it is noted that at point a there is a stress drop $(\Delta\sigma_p)$ up to the point a', which has its value decreased to nullity at point b. The stress variation $(\Delta\sigma_p)$ decreases until the unmovable point (b) to the anchorage due to the friction existing in the cable-sheath assembly. Thus, there are two relevant unknowns: the acting stress $(\sigma_{p,R})$ at the undisplaceable point (b) and the distance (x_R) from the active anchorage. With at least one of these unknowns, applying geometric relationships and the consequent quantification of stresses in each analysis section becomes possible. However, in short beams or even in some cases of active anchoring at both ends (situation B, Figure 3b), despite the friction in the cable-sheath assembly, the stress reduction $(\Delta\sigma_p)$ does not reach nullity in the point b, and the distance x_R is known and equal to ℓ. Therefore, the value of $\sigma_{p,R}$, and the stresses in the corresponding analysis sections are identified by applying geometric relations.
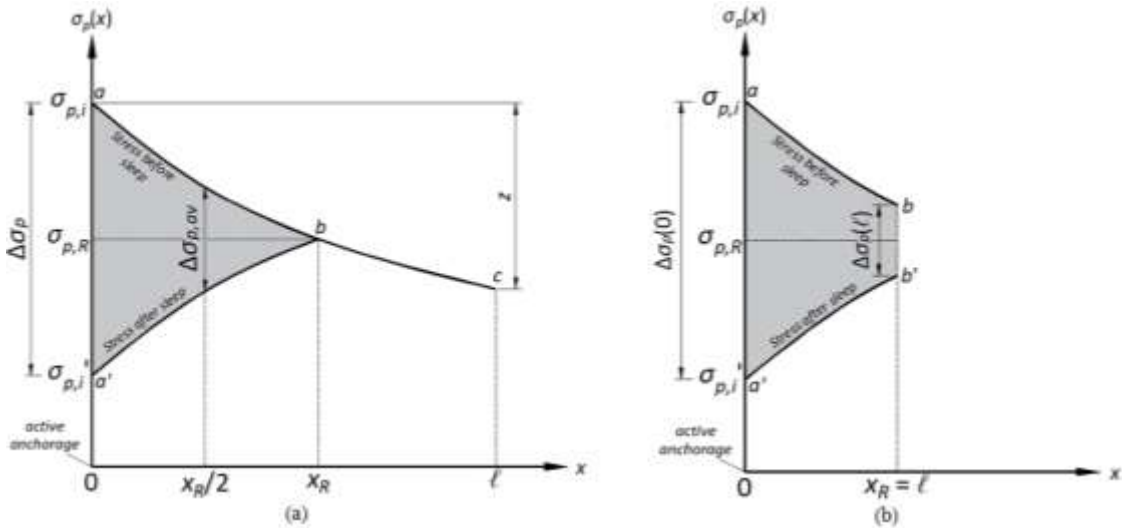
Figure 3. Stress development along the cable in the anchoring process: Situation A (a) and B (b). Source: Adapted from Bastos (2019b).

Assuming that the frictional stresses acting on stretching and slipping are of the same intensity for situation A (Figure 3a), both Naaman (2012) and Dolan and Hamilton (2019) admit that curves *a-b* and *a'-b* are line segments that form the isosceles triangle *a-b-a'*. Therefore, the stress drop ($\Delta\sigma_p$) in the active anchorage is given by Equation 2 and the average stress loss ($\Delta\sigma_{p,av}$) in section $x = x_R$ is given by Equation 3.

$$\Delta\sigma_p = \sigma_{p,i} - \sigma_{p,i}' \Rightarrow \Delta\sigma_p = 2 \cdot (\sigma_{p,i} - \sigma_{p,R}) \Rightarrow \Delta\sigma_p = 2 \cdot \Delta\sigma_{p,av} \tag{2}$$

$$\boldsymbol{\Delta\sigma_{p,av} = \sigma_{p,i} - \sigma_{p,R}} \tag{3}$$

Where, $\sigma_{p,i}'$: Stress in active reinforcement after slipping of the anchor (section $x = 0$).

Using the Taylor expansion, Naaman (2012) applies Equation 1 to Equation 3, disregarding the higher-order terms, as presented in Equation 4.

$$\Delta\sigma_{p,av} = \sigma_{p,i} - \sigma_{p,i} \cdot e^{-\lambda \cdot x_R} \Rightarrow \Delta\sigma_{p,av} = \sigma_{p,i} - \sigma_{p,i} \cdot (1 - \lambda \cdot x_R) = \sigma_{p,i} \cdot \lambda \cdot x_R \tag{4}$$

Considering that the active reinforcement presents a constant shortening along the stretch x_R, the average loss ($\Delta\varepsilon_{p,av}$) of deformation is given by the ratio between the slip of the anchorage (δ) and the abscissa x_R. Therefore, applying Hooke's Law, Naaman (2012) proposes a second expression (Equation 5) to quantify the average stress loss $\Delta\sigma_{p,av}$.

$$\Delta\sigma_{p,av} = \Delta\varepsilon_{p,av} \cdot E_p \Rightarrow \Delta\sigma_{p,av} = \frac{\delta}{x_R} \cdot E_p \tag{5}$$

Where, E_p: Modulus of elasticity of active reinforcement steel.

Finally, equating Equation 4 with Equation 5, Naaman (2012) determines the distance x_R through Equation 6.

$$\sigma_{p,i} \cdot \lambda \cdot x_R = \frac{\delta}{x_R} \cdot E_p \Rightarrow x_R = \sqrt{\frac{\delta \cdot E_p}{\sigma_{p,i} \cdot \lambda}} \tag{6}$$
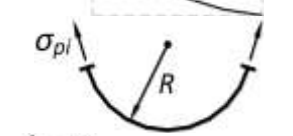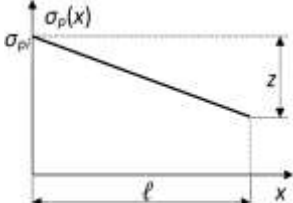
It is possible to note that x_R depends on the initial prestressing stress ($\sigma_{p,i}$) and friction and curvature of the cables (λ). However, Equation 6 is only valid when λ is constant over a considered curvature and x_R is not greater than the length of the curvature relative to its λ (Naaman, 2012; Dolan & Hamilton, 2019). Recommended values of λ are shown in Table 1.

(Table 1). In that case, the Precast/Prestressed Concrete Institute (PCI, 2017) recommends Equation 7 to determine x_R.

$$x_R = \sqrt{\frac{\delta \cdot E_p}{(z/\ell)}} \tag{7}$$

Where, ℓ: span or a known distance along the cable; z: the stress loss over distance ℓ.

Table 1. Recommended values for λ and x_R to typical passive reinforcement profiles.

Profile	Description	λ	$x_R \leq \ell$
Linear		k	$x_R = \sqrt{\dfrac{\delta \cdot E_p}{\sigma_{p,i} \cdot k}}$
Parabolic		$2 \cdot \left(\dfrac{\mu \cdot a}{b^2}\right) + k$	$x_R = \sqrt{\dfrac{\delta \cdot E_p}{\sigma_{p,i} \cdot \lambda}}$
Circular		$\dfrac{\mu}{R} + k$	$x_R = \sqrt{\dfrac{\delta \cdot E_p}{\sigma_{p,i} \cdot \lambda}}$
Any shape or combination of shapes (approximate model over a length ℓ)		$\left(\dfrac{z}{\ell}\right) \cdot \dfrac{1}{\sigma_{p,i}}$	$x_R = \sqrt{\dfrac{\delta \cdot E_p}{\left(z/\ell\right)}}$

Source: Adapted from Naaman (2012).

Suppose there are different values of λ, and the distance x_R is greater than the length of a given curvature In situation B (Figure 3b), Naaman (2012) admits that the region a-b-b'-a' corresponds to an isosceles trapezoid, whose area is given by Equation 8. Therefore, the variation ($\Delta\sigma_p$) of voltage at position $x = \ell$ can be written using Equation 9.

$$\text{Loss area} = \left[\frac{\Delta\sigma_p(0) + \Delta\sigma_p(\ell)}{2}\right] \cdot \ell = \delta \cdot E_p \tag{8}$$

$$\Delta\boldsymbol{\sigma_p(\ell)} = \Delta\boldsymbol{\sigma_p(0)} - \boldsymbol{2} \cdot [\boldsymbol{\sigma_{p,i}} - \boldsymbol{\sigma_p(\ell)}] \tag{9}$$

Ignoring the higher-order terms, the stress (σ_p) at position $x = \ell$ is simplified through Taylor expansion, as expressed in Equation 10.

$$\sigma_p(\ell) = \sigma_{p,i} \cdot e^{-\lambda \cdot \ell} \Rightarrow \sigma_p(\ell) = \sigma_{p,i} \cdot (1 - \lambda \cdot \ell) = \sigma_{p,i} - \sigma_{p,i} \cdot \lambda \cdot \ell \tag{10}$$

Substituting Equation 10 in Equation 9 and adjusting the term $\Delta\sigma_p(0)$ through Equation 8, it is possible to obtain the stress variation at position $x = \ell$ and consequently the stress $\sigma_{p,R}$, both represented by Equation 11.

$$\Delta\sigma_p(\ell) = \frac{\delta \cdot E_p}{\ell} - \sigma_{p,i} \cdot \lambda \cdot \ell \therefore \sigma_{p,R} = \sigma_p(\ell) - \frac{\Delta\sigma_p(\ell)}{2} \tag{11}$$

Carvalho (2012) disregards the isosceles triangle a-b-a' (Figure 3a), assuming the area between two curves in situation A, as illustrated in Figure 4a.
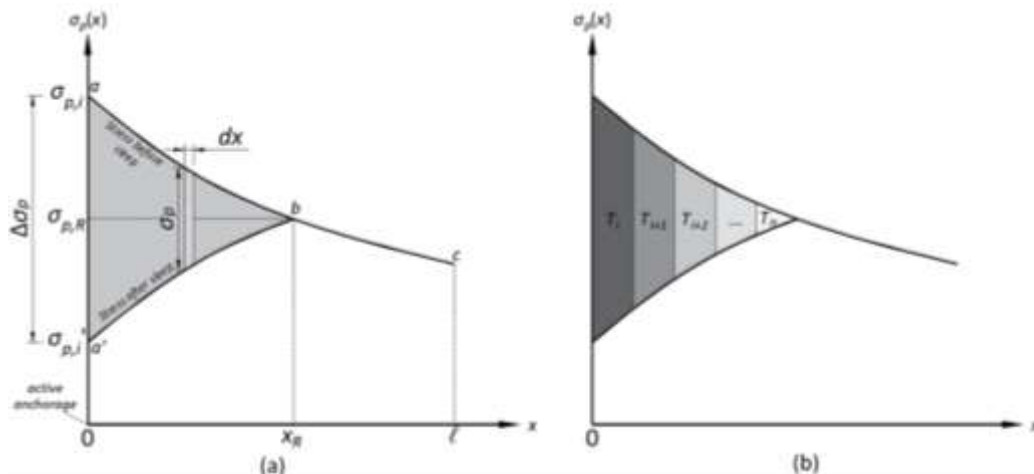
Figure 4. Area between curves (a) and division of the domain of integration into areas of trapezoids (b). Source: Adapted from Carvalho (2012).

The area (Ω_R) of the region *a-b-a'* is given by Equation 12.

$$\int_0^{x_R} \sigma_p \, dx = \delta \cdot E_p \Rightarrow \Omega_R = \delta \cdot E_p \tag{12}$$

Hence, the unknown consists of the distance x_R needed to produce an area between curves equal to Ω_R. Carvalho (2012) proposes dividing the integration domain into arbitrary sections whose areas correspond to isosceles trapezoids (Figure 4b). Due to the very remote probability that the sum of these areas will result in a value equal to Ω_R, attempts are made to identify the sections immediately before ($x = x_{R-1}$) and after ($x = x_{R+1}$) to the undisplaceable point ($x = x_R$). The area (Ω_n) is estimated for each iteration through Equation 13.

$$\Omega_n = \sum_{i=1}^{n-1} \{[(\sigma_{p,i} - \sigma_{p,n}) + (\sigma_{p,i+1} - \sigma_{p,n})] \cdot (x_{i+1} - x_i)\} \tag{13}$$

Once the coordinates of the immediately previous ($x_{R-1}, \sigma_{p,R-1}$) and posterior ($x_{R+1}, \sigma_{p,R+1}$) sections are known, the formulation of the area Ω_R can be rewritten through Equation 14, assuming that Ω_p (Figure 5) corresponds to the area of a parallelogram and Ω_t (Figure 5) to the area of an isosceles triangle.

$$\Omega_R = \Omega_{R-1} + \Omega_p + \Omega_t =$$
$$= \Omega_{R-1} + \left[2 \cdot \overbrace{(\sigma_{p,R-1} - \sigma_{p,R})}^{\Delta\sigma_1} \cdot x_{R-1} \right] + \left[\overbrace{(\sigma_{p,R-1} - \sigma_{p,R})}^{\Delta\sigma_1} \cdot \overbrace{(x_R - x_{R-1})}^{\Delta x_1} \right] \tag{14}$$
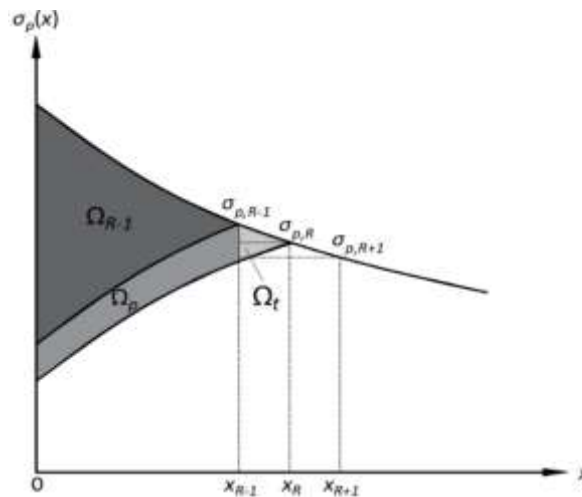

Figure 5. Definition of the areas (Ω_p e Ω_t) e similarity of triangles. Source: Adapted from Carvalho (2012).

By similarity of triangles, the formulation of Δx_1 is in Equation 15.

$$\frac{\overbrace{(x_R - x_{R-1})}^{\Delta x_1}}{\underbrace{(x_{R+1} - x_{R-1})}_{\Delta x_2}} = \frac{\overbrace{(\sigma_{p,R-1} - \sigma_{p,R})}^{\Delta\sigma_1}}{\underbrace{(\sigma_{p,R-1} - \sigma_{p,R+1})}_{\Delta\sigma_2}} \Rightarrow \Delta x_1 = \frac{\Delta x_2}{\Delta\sigma_2} \cdot \Delta\sigma_1 \tag{15}$$

In situation A (Figure 3a), to determine the variation $\Delta\sigma_1$, Equation 15 is substituted in Equation 14, resulting in a polynomial of degree two, as presented in Equation 16.

Situation A: $\left(\dfrac{\Delta x_2}{\Delta x_1}\right) \cdot \Delta\sigma_1{}^2 + (2 \cdot x_{R-1}) \cdot \Delta\sigma_1 + (\Omega_{R-1} - \Omega_R) = 0 \tag{16}$

As in situation B (Figure 3b) there is no term Δx_2, since the posterior section ($x = x_{R+1}$) is non-existent, Equation 16 is rewritten in Equation 17 only for this situation.

Situation B: $\Delta\sigma_1 = \dfrac{\Omega_R - \Omega_{R-1}}{2 \cdot x_{R-1}} \tag{17}$

Once the value of $\Delta\sigma_1$ has been calculated, it becomes possible to determine the stress $(\sigma_{p,R})$ at the undisplaceable point $(x = x_R)$ to the anchorage. Therefore, the stresses $[\sigma_p{}'(x)]$ after the loss by deformation of the anchor in each section are given by Equation 18.

$$\sigma_p{}'(x) = \sigma_p(x) - \left\{2 \cdot \left[\sigma_p(x) - \sigma_{p,R-1}\right] + \Delta\sigma_1\right\} \quad 0 \le x \le x_R \tag{18}$$

The quantification of the loss by deformation of the anchor idealized by Marconato and Sartorti (2015) starts from the same area premise between two curves Carvalho (2012) proposed. However, contrary to the division of the area Ω_n into trapezoids at each iteration, Marconato and Sartorti (2015) use the Gauss formulation (Equation 19) for the area of an irregular polygonal, represented by Figure 6, where Ω_n corresponds to twice the hatched area a-b-c.
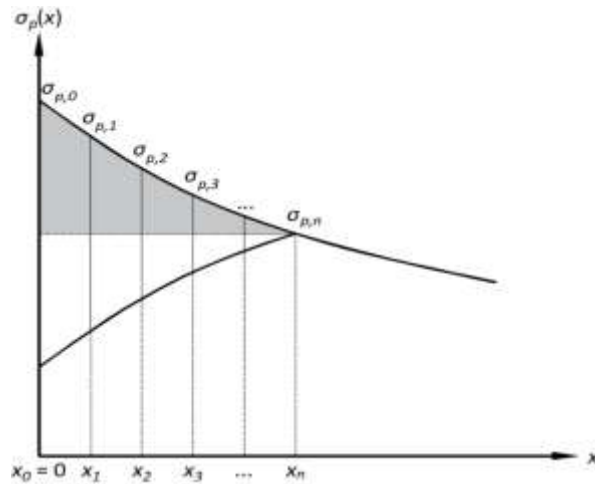

Figure 6. Area of an irregular polygonal by the Gaussian formulation.

$\sum 1$ products	x / σ	$\sum 2$ products
	x_0 ╳ $\sigma_{p,0}$	
$x_1 \cdot \sigma_{p,0}$	x_1 ╳ $\sigma_{p,1}$	$x_0 \cdot \sigma_{p,1}$
$x_2 \cdot \sigma_{p,1}$	x_2 ╳ $\sigma_{p,2}$	$x_1 \cdot \sigma_{p,2}$
...	... ╳ ...	...
...	x_n ╳ $\sigma_{p,n}$	...
$x_0 \cdot \sigma_{p,n}$	x_0 ╳ $\sigma_{p,n}$	$x_n \cdot \sigma_{p,n}$
$x_1 \cdot \sigma_{p,n}$	x_1 ╳ $\sigma_{p,0}$	$x_0 \cdot \sigma_{p,0}$
$\sum 1$		$\sum 2$

$$\Omega_n = 2 \cdot \left(\frac{\sum 1 - \sum 2}{2}\right) = \sum 1 - \sum 2 \tag{19}$$

From Figure 6, the area of the sections S_1 $(x = x_1)$ and S_2 $(x = x_2)$ are given by Equation 20.

$\sum 1$	x / σ	$\sum 2$
	x_0 ╳ $\sigma_{p,0}$	
$x_1 \cdot \sigma_{p,0}$	x_1 ╳ $\sigma_{p,1}$	$x_0 \cdot \sigma_{p,1} = 0$
$x_0 \cdot \sigma_{p,1} = 0$	x_0 ╳ $\sigma_{p,1}$	$x_1 \cdot \sigma_{p,1}$
$x_0 \cdot \sigma_{p,1} = 0$	x_0 ╳ $\sigma_{p,0}$	$x_0 \cdot \sigma_{p,0} = 0$
$\sum 1$		$\sum 2$

$$\Omega_1 = x_1 \cdot \sigma_{p,0} - x_1 \cdot \sigma_{p,1}$$

$\sum 1$	x / σ	$\sum 2$
	x_0 ╳ $\sigma_{p,0}$	
$x_1 \cdot \sigma_{p,0}$	x_1 ╳ $\sigma_{p,1}$	$x_0 \cdot \sigma_{p,1} = 0$
$x_2 \cdot \sigma_{p,1}$	x_2 ╳ $\sigma_{p,2}$	$x_1 \cdot \sigma_{p,2}$
$x_0 \cdot \sigma_{p,2} = 0$	x_0 ╳ $\sigma_{p,2}$	$x_2 \cdot \sigma_{p,2}$
$x_0 \cdot \sigma_{p,2} = 0$	x_0 ╳ $\sigma_{p,1}$	$x_0 \cdot \sigma_{p,1} = 0$
$\sum 1$		$\sum 2$

$$\Omega_2 = \left(x_1 \cdot \sigma_{p,0} + x_2 \cdot \sigma_{p,1}\right) - \left(x_1 \cdot \sigma_{p,2} + x_2 \cdot \sigma_{p,2}\right)$$

(20)

Replacing the common term $(x_1 \cdot \sigma_{p,0})$ of the area Ω_1 in area Ω_2, there is the new area of the section S_2 $(x = x_2)$ represented by Equation 21.

$$\Omega_2 = \Omega_1 + x_1 \cdot \sigma_{p,1} + x_2 \cdot \sigma_{p,1} - x_1 \cdot \sigma_{p,2} - x_2 \cdot \sigma_{p,2} \Rightarrow$$
$$\Omega_2 = \Omega_1 + (x_1 + x_2) \cdot (\sigma_{p,1} - \sigma_{p,2}) \tag{21}$$

Therefore, rewriting Equation 21 to cover all sections of analysis, it is possible to obtain the formulation presented in Equation 22.

$$\Omega_n = \Omega_{n-1} + (x_{n-1} + x_n) \cdot (\sigma_{p,n-1} - \sigma_{p,n}) \tag{22}$$

Once the coordinates of the immediately preceding $(x_{R-1}, \sigma_{p,R-1})$ and posterior $(x_{R+1}, \sigma_{p,R+1})$ sections have been determined, Marconato and Sartorti (2015) determine the position of the unmovable point $(x_R, \sigma_{p,R})$ for the two situations (A and B) presented in Table 2.

Table 2. Different situations in determining the position of the non-displaceable point to the anchorage.

Situation A	Situation B
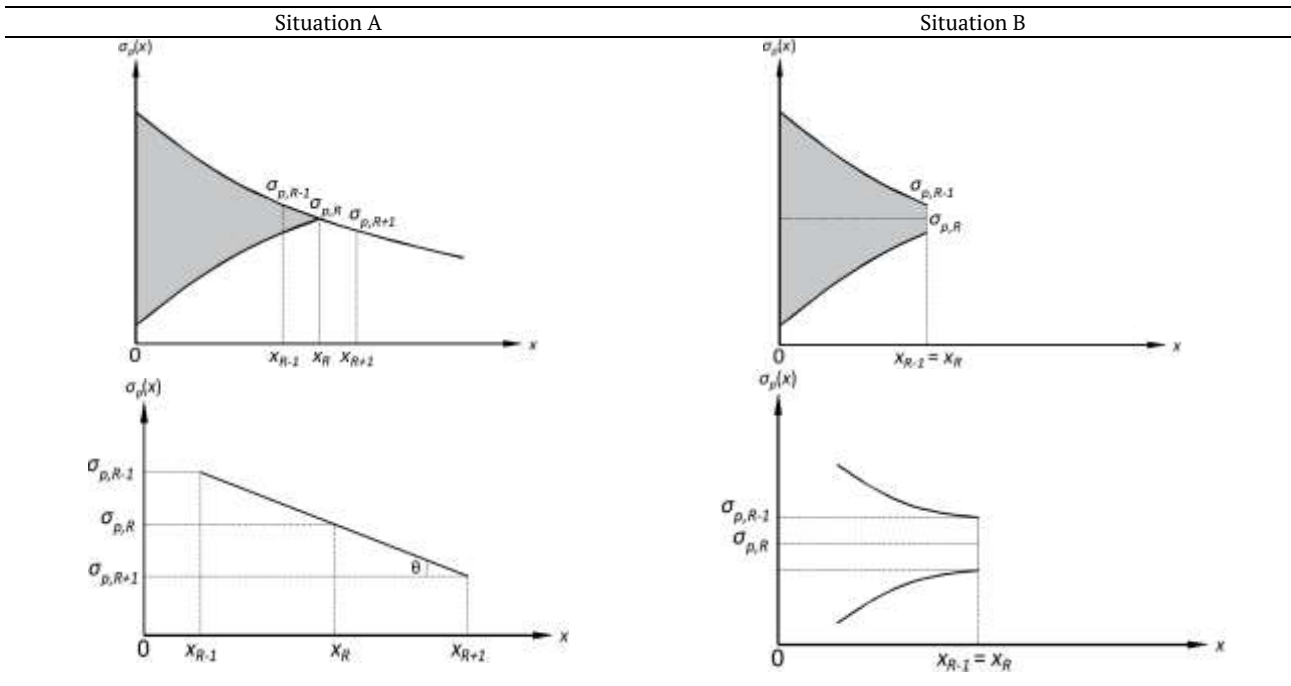
In situation A, by the similarity of triangles, the stress $(\sigma_{p,R})$ at the undisplaceable point $(x = x_R)$ is given by Equation 23.

$$\sigma_{p,R} = \sigma_{p,R-1} + (x_R - x_{R-1}) \cdot \overbrace{\left(\frac{\sigma_{p,R+1} - \sigma_{p,R-1}}{x_{R+1} - x_{R-1}} \right)}^{\tan \theta} \tag{23}$$

However, x_R is still unknown. To determine its value, Equation 23 is substituted in Equation 22, as shown in Equation 24, noting that $\sigma_{p,n} = \sigma_{p,R}$.

$$\Omega_R = \Omega_{R-1} + (x_{R-1} + x_R) \cdot \{\sigma_{p,R-1} - [\sigma_{p,R-1} + (x_R - x_{R-1}) \cdot \tan \theta]\} \Rightarrow$$
$$\Rightarrow x_R = \sqrt{x_{R-1}^2 + \frac{\Omega_{R-1} - \Omega_R}{\tan \theta}} \tag{24}$$

In situation B, x_R is known and equal to x_{R-1}. Assuming this premise, Equation 22 is rewritten by isolating the term $\sigma_{p,R}$, as shown in Equation 25.

$$\Omega_R = \Omega_{R-1} + (x_{R-1} + x_{R-1}) \cdot (\sigma_{p,R-1} - \sigma_{p,R}) \Rightarrow \sigma_{p,R} = \sigma_{p,R-1} + \frac{\Omega_{R-1} - \Omega_R}{2 \cdot x_{R-1}} \tag{25}$$

Finally, the stresses $[\sigma_p'(x)]$ after the loss by deformation of the anchor in each section are given by Equation 26.

$$\sigma_p'(x) = \sigma_p(x) - \{2 \cdot [\sigma_p(x) - \sigma_{p,R}]\} = 2 \cdot \sigma_{p,R} - \sigma_p(x) \quad 0 \le x \le x_R \tag{26}$$

Once the concepts of prestressing losses are presented and the methodologies for quantifying the loss due to anchorage deformation, it is necessary to associate them with the main objective of the work, consolidating in the computational implementation of the alternative method of Marconato and Sartorti (2015). Therefore, the necessary data insertion steps to obtain the final stress values $[\sigma_p'(x)]$ will be presented in the following topics. The computational tool, vProt, was coded on the Microsoft Office Excel 365 2019 platform through the Visual Basic for Applications (VBA) language. Although the software has been programmed to determine all prestressing losses in a prestressed concrete element, it should be noted that only the information required to quantify the anchor slip loss will be presented in this work.

In order to cover the two situations (A and B, Figure 3) idealized by Marconato and Sartorti (2015), two beams (I and II) of the same cross-section will be simulated; however, they have different spans and cable paths. In Figure 7, the respective cross-section is illustrated. In Figure 8 and Figure 9, the static scheme and the longitudinal section of beams I and II are respectively shown.
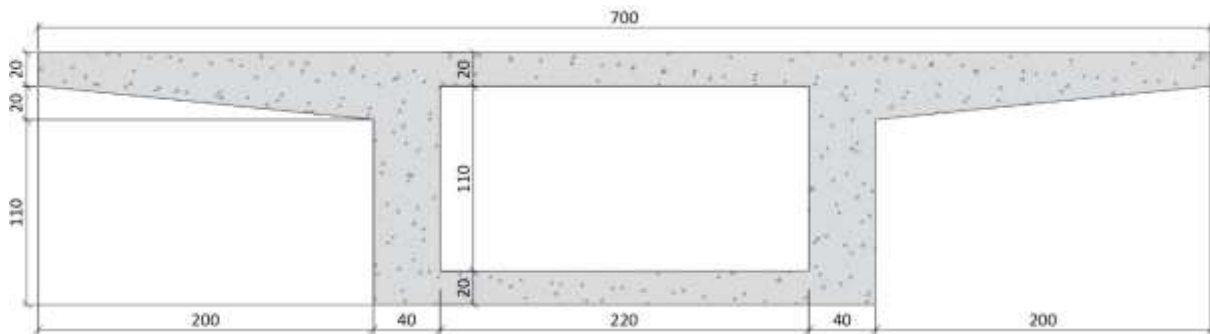

Figure 7. Cross-section of beams I and II (dimensions in centimeters). Source: Sartorti (2018).
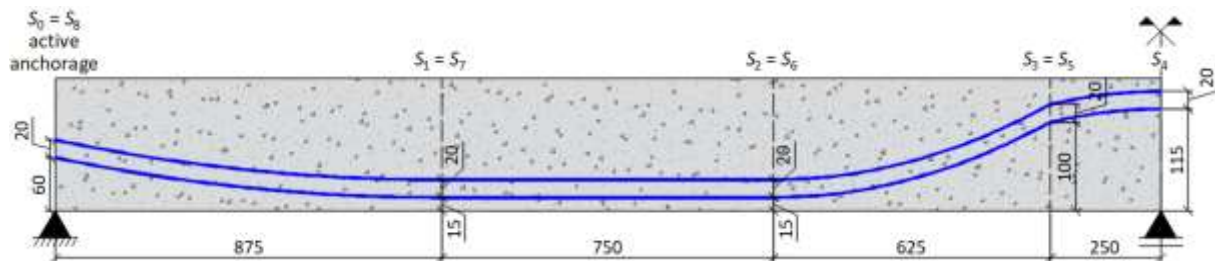

Figure 8. Static diagram and longitudinal section of beam I (dimensions in centimeters). Source: Adapted from Sartorti (2018).
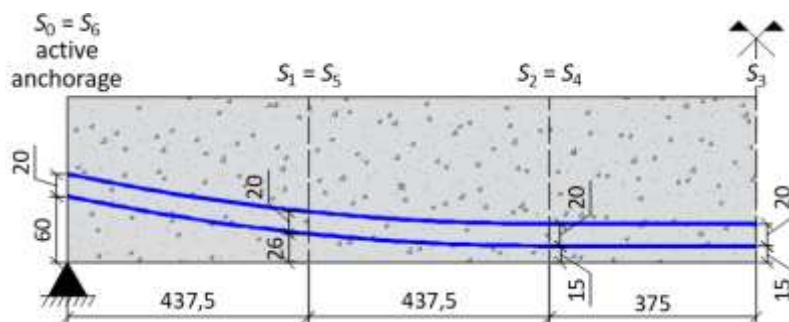

Figure 9. Static diagram and longitudinal section of beam II (dimensions in centimeters). Source: Adapted from Sartorti (2018).

It is observed that the anchorage is active at both ends of beams I and II. Furthermore, the span of beam II is relatively smaller than that of beam I, in order to avoid creating the fixed point, thus falling into situation B. It is noteworthy that the position of the representative cable is in the center of gravity of the total set of cables, whose layout has a parabolic geometry in the non-straight sections.

In calculating the friction loss (Equation 1), the values of deviation angles (α) in parabolic curvatures are quantified through Equation 27.

$$\alpha = \tan^{-1}\left(\frac{2 \cdot f}{\ell}\right) \tag{27}$$

Where, f: cable drop in the section in question; ℓ: is the total length of the section.

The vProt software automatically determines these curvatures according to information pre-established by the user. Their values are printed in Table for both beams I and II.

Table 3. Deviation angles between the anchorage and the x-abscissa point (beams I and II).

Section	Beam I			Beam II		
	ℓ (m)	f (cm)	α (rad)	ℓ (m)	f (cm)	α (rad)
$S_0 - S_1$	8.750	45.00	0.1025	4.375	33.75	0.1531
$S_1 - S_2$	7.500	0.000	0.0000	4.375	11.25	0.0514
$S_2 - S_3$	6.250	85.00	0.2656	3.750	0.000	0.0000
$S_3 - S_4$	2.500	15.00	0.1194	-	-	-

In addition to geometry, some prior information regarding prestressing parameters, must be reported to quantify anchor slip loss effectively, including:

- Coefficient of friction between the wire and the duct for determining friction loss: $\mu = 0.20$;
- Slip of the anchorage wedge, that is, the distance the anchorage wedge slides towards the "interior" of the concrete member: $\delta = 8\ mm$;
- Ultimate characteristic strength of the prestressing steel: $f_{ptk} = 1900\ MPa$; this strength refers to low relaxation (LR) prestressing steels supplied by manufacturers.

The vProt software calculates the initial stress ($\sigma_{p,i}$) following the recommendations of item 9.6.1.2.1.b of ABNT (2014), whose wording is as follows: "The stress $\sigma_{p,i}$ of the prestressing reinforcement at the output of the tensile device must respect the limits of $0.74 f_{ptk}$ and $0.87 f_{pyk}$ for steels of the normal relaxation class, and $0.74 f_{ptk}$ and $0.82 f_{pyk}$ for steels of the low relaxation class". A low-relaxation steel (LR) is used, then the initial stress ($\sigma_{p,i}$) of prestressing is given by Equation 28. For computational purposes, the lower value between the two limits is adopted. However, it should be noted that, technically, both ($0.74 f_{ptk}$ and $0.82 f_{pyk}$) correspond to the same value.

$$\sigma_{p,i} \leq \begin{cases} 0.74 \cdot f_{ptk} = 0.74 \cdot 1900 = 1406.0\ MPa \\ 0.82 \cdot f_{pyk} = 0.82 \cdot 0.90 \cdot 1900 = 1402.2\ MPa \end{cases} \tag{28}$$

Where, f_{pyk}: characteristic value of conventional yield strength equal to $0.90 \cdot f_{ptk}$.

Results and discussion

Since the friction loss precedes the moment of anchoring, the vProt software determines the stresses $[\sigma_p(x)]$ after stretching the cables in each section of the active reinforcement, according to Equation 1, presented above. Their values are sown in Table 4.

Table 4. Stresses [σ_p (x)] after the friction loss in each section of active reinforcement.

Section	Beam I				Beam II			
	x (m)	$\sum \alpha$ (rad)	$e^{-\lambda \cdot x}$	$\sigma_p(x)$ (MPa)	x (m)	$\sum \alpha$ (rad)	$e^{-\lambda \cdot x}$	$\sigma_p(x)$ (MPa)
S_0	0.000	0.0000	1.0000	1402.2	0.000	0.0000	1.0000	1402.2
S_1	8.750	0.1025	0.9627	1349.9	4.375	0.1531	0.9614	1348.1
S_2	16.25	0.1025	0.9484	1329.8	8.750	0.2045	0.9433	1322.7
S_3	22.50	0.3681	0.8882	1245.4	12.50	0.2045	0.9362	1312.8
S_4	25.00	0.4875	0.8629	1209.9	-	-	-	-

As long as the methodology proposed by Marconato and Sartorti (2015) includes simplified equations, the estimate of Ω_n is calculated sequentially until the immediately preceding (x_{R-1}, $\sigma_{p,R-1}$) and posterior (x_{R+1}, $\sigma_{p,R+1}$) sections are identified. The area Ω_R was obtained by Equation 29.

$$\Omega_R = \delta \cdot E_p = 0.008 \cdot 2.0 \cdot 10^8 = 1.6 \cdot 10^6\ kN/m \tag{29}$$

Therefore, the vProt software produced the values for beam I, contained in Table .

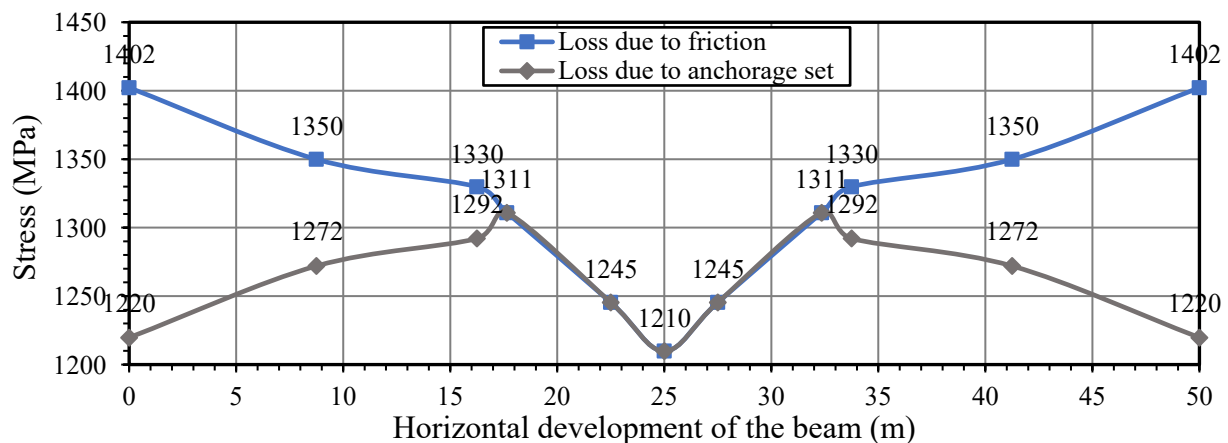**Table 5.** Anchor slip loss on the beam I (alternative methodology).

Section	x (m)	$x_{n-1} + x_n$ (m)	$\sigma_p(x)$ (MPa)	$\frac{\sigma_{p,n-1} + \sigma_{p,n}}{2}$ (MPa)	Ω_n (kN/m)	$\sigma_p'(x)$ (MPa)
S_0	0.000	0.000	1402.2	0.00	0.0000	1219.7
S_1	8.750	8.750	1349.9	52.3	457476	1272.0
S_2	16.25	25.00	1329.8	20.1	959918	1292.1
S_3	22.50	38.75	1245.4	84.5	423255	1245.4
S_4	25.00	47.50	1209.9	-	-	1209.9

It is possible to notice that the anchoring point ($x = x_R$) is located between sections S_2 and S_3, then they are in situation A. Therefore, from Marconato and Sartorti (2015), it is possible to state Equation 30 and Equation 31, the position of the undisplaceable point (x_R) and the acting stress ($\sigma_{p,R}$), respectively.

$$x_R = \sqrt{x_{R-1}^2 + \frac{\Omega_{R-1} - \Omega_R}{\tan\theta}} = \sqrt{16.25^2 + \frac{959918 - 1.6 \cdot 10^6}{-13504}} = 17.65 \; m \tag{30}$$

$$\sigma_{p,R} = \sigma_{p,R-1} + (x_R - x_{R-1}) \cdot \tan\theta = 1329800 + (17.65 - 16.25) \cdot (-13504) = 1310.9 \; MPa \tag{31}$$

The stresses [$\sigma_p'(x)$] after the loss by accommodation of the anchor in the sections prior to the undisplaceable point ($x = x_R$) were calculated using Equation 26, presented above. Their results are shown in the last column of Table , together with the stresses [$\sigma_p'(x)$] in the later sections, whose values remained equal to the friction loss. Figure 10 graphically illustrates the loss of prestressing after friction and slippage of the anchor on beam I.

Figure 10. Graphic representation of the loss of prestressing by friction and deformation of the anchor (beam I).

Analogously to beam I, Table contains the results of beam II using the alternative methodology of Marconato and Sartorti (2015), quantified by the vProt software.

Table 6. Anchor slip loss on the beam II (alternative methodology).

Section	x (m)	$x_{n-1} + x_n$ (m)	$\sigma_p(x)$ (MPa)	$\frac{\sigma_{p,n-1} + \sigma_{p,n}}{2}$ (MPa)	Ω_n (kN/m)	$\sigma_p'(x)$ (MPa)
S_0	0.000	0.0000	1402.2	0.00	0.00000	1157.8
S_1	4.375	4.3750	1348.1	54.1	236803	1211.9
S_2	8.750	13.125	1322.7	25.4	570268	1237.3
S_3	12.50	21.250	1312.8	9.90	780279	1247.2

It is possible to notice that in this beam, the anchoring point ($x = x_R$) is located after section S_3. Therefore, the variation ($\Delta\sigma_p$) of stress does not reach null since beam II includes active anchoring at both ends, falling into situation B. Therefore, the abscissa x_R is known and equal to 12.50 m, and the average stress ($\sigma_{p,R}$) is given by Equation 32.

$$\sigma_{p,R} = \sigma_{p,R-1} + \frac{\Omega_{R-1} - \Omega_R}{2 \cdot x_{R-1}} = 1312800 + \frac{780279 - 1.6 \cdot 10^6}{2 \cdot 12.50} = 1280.0 \; MPa \tag{32}$$

As in beam I, the stresses $[\sigma_p'(x)]$ after the anchorage accommodation loss were calculated using Equation 26, presented above. Its results are presented in the last column of Table . Figure 11 graphically illustrates the loss of prestressing after friction and slippage of the anchor in beam II.
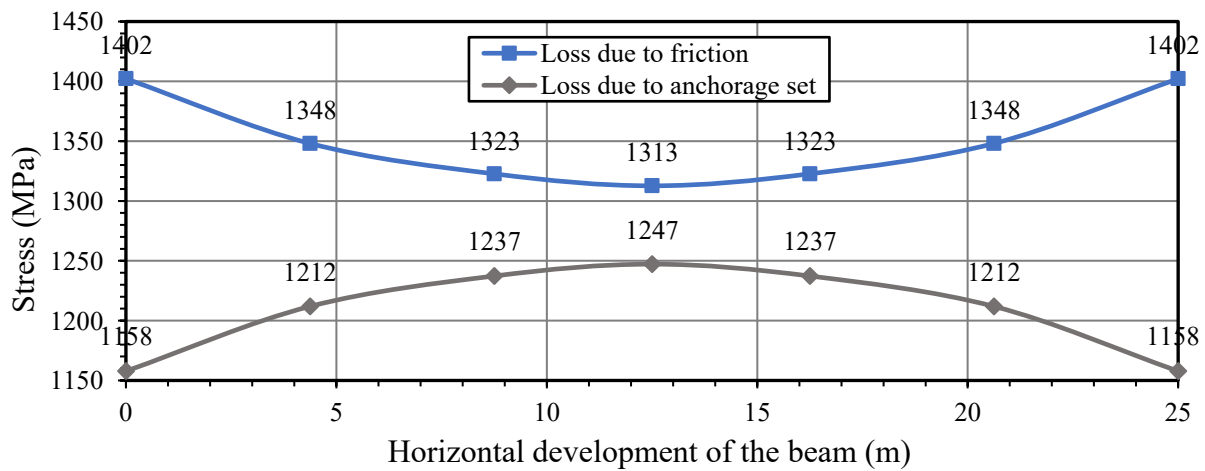

Figure 11. Graphic representation of the loss of prestressing by friction and deformation of the anchor (beam II).

To verify the effectiveness of Marconato and Sartorti's (2015) alternative method, we chose to measure it with the two conventional methodologies exposed in item "Material and Methods". The results of beam I are shown in Table .

Table 7. Measurement of the Marconato and Sartorti (2015) method with conventional methodologies (beam I).

Section	[1]M&S $\sigma_p'(x)$ (MPa)	[2]N and D&H $\sigma_p'(x)$ (MPa)	% difference (%)	[1]M&S $\sigma_p'(x)$ (MPa)	[3]C $\sigma_p'(x)$ (MPa)	% difference (%)
S_0	1219.7	1263.8	3.62	1219.7	1219.7	0.00
S_1	1272.0	1316.1	3.47	1272.0	1272.0	0.00
S_2	1292.1	1329.8	2.92	1292.1	1292.1	0.00
S_3	1245.4	1245.4	0.00	1245.4	1245.4	0.00
S_4	120.99	120.99	0.00	120.99	120.99	0.00

[1]M&S: Marconato and Sartorti (2015); [2]N and D&H: Naaman (2012) and Dolan and Hamilton (2019); [3]C: Carvalho (2012).

Table shows a slight divergence of the alternative methodology in relation to the method of Naaman (2012) and Dolan and Hamilton (2019), in which the abscissa (x_R) of the unmovable point is between sections S_1 and S_2, as evidenced in Equation 33. Therefore, the stress ($\sigma_{p,R}$) also assumes a different value, as shown in Equation 34.

$$x_R = \sqrt{\frac{\delta \cdot E_p}{(z/\ell)}} = \sqrt{\frac{0.008 \cdot 2.0 \cdot 10^8}{\left(192300/25.00\right)}} = 14.42 \; m \tag{33}$$

$$\sigma_{p,R} = \sigma_{p,i} \cdot (1 - \lambda \cdot x_R) = 1402200 \cdot (1 - 3.4213 \cdot 10^{-3} \cdot 14.42) = 1333.0 \; MPa \tag{34}$$

The beam II measurements are shown in Table .

Table 8. Measurement of the Marconato and Sartorti (2015) method with conventional methodologies (beam II)

Section	[1]M&S $\sigma_p'(x)$ (MPa)	[2]N and D&H $\sigma_p'(x)$ (MPa)	% difference (%)	[1]M&S $\sigma_p'(x)$ (MPa)	[3]C $\sigma_p'(x)$ (MPa)	% difference (%)
S_0	1157.8	1181.8	2.07	1157.8	1157.8	0.00
S_1	1211.9	1235.9	1.98	1211.9	1211.9	0.00
S_2	1237.3	1261.3	1.94	1237.3	1237.3	0.00
S_3	1247.2	1271.2	1.93	1247.2	1247.2	0.00

[1]M&S: Marconato and Sartorti (2015); [2]N and D&H: Naaman (2012) and Dolan & Hamilton (2019); [3]C: Carvalho (2012).

By the method of Naaman (2012) and Dolan and Hamilton (2019), the variation ($\Delta\sigma_p$) of stress in section $x = \ell$ was obtained using Equation 35 and the average stress ($\sigma_{p,R}$) by Equation 36, showing a small divergence in relation to the alternative methodology of Marconato and Sartorti (2015).

$$\Delta\sigma_p(\ell) = \frac{\delta \cdot E_p}{\ell} - \sigma_{p,i} \cdot \lambda \cdot \ell = \frac{0.008 \cdot 2.0 \cdot 10^8}{12.50} - 1402200 \cdot 5.2714 \cdot 10^{-3} \cdot 12.50 = 35.6 \, MPa \tag{35}$$

$$\sigma_{p,R} = \sigma_p(\ell) - \frac{\Delta\sigma_p(\ell)}{2} = (1402200 - 1402200 \cdot 5.2714 \cdot 10^{-3} \cdot 12.50) - \frac{35.6}{2} = 1292.0 \, MPa \tag{36}$$

As the alternative methodology by Marconato and Sartorti (2015) was conceived from Carvalho (2012), there is no divergence between both methods. It should be noted that the methodology from Carvalho (2012) configure better accuracy in the results since there is a stratification of the longitudinal section, representing the area Ω_R more reliably. Thus, the greater the number of sections, the more realistic the loss quantification due to anchorage deformation will be. Although the methodology of Naaman (2012) and Dolan and Hamilton (2019) has practical applicability, the results differ from those quantified by Marconato and Sartorti (2015) and Carvalho (2012). It occurs because the area Ω_R does not represent a perfect isosceles triangle and trapezoid for situations A and B, respectively, as shown in Figure 10 and 11.

Conclusion

After simulating two beams representing different stress development scenarios (A and B) along the cable, the following observations were made: The alternative method by Marconato and Sartorti (2015) accurately quantifies prestressing loss from anchorage deformation in post-tensioning, showing minimal differences compared to conventional methods. The software is reliable, providing users with flexibility in analysis and cable development. Both Carvalho (2012) and Marconato and Sartorti (2015) offer more realistic results than Naaman (2012) and Dolan and Hamilton (2019). Marconato and Sartorti's (2015) alternative method presents a simpler formulation for quantifying Ω_n, eliminating the need for dividing the integration domain into trapezoids.

Acknowledgements

References

Abdel-Jaber, H., & Glisic, B. (2018). Monitoring of long-term prestress losses in prestressed concrete structures using fiber optic sensors. *Structural Health Monitoring*, *18*, 254-269. DOI: https://doi.org/10.1177/1475921717751870

Araújo, D. L., Sales, M. W. R., Silva, R. P. M., Antunes, C. F. M., & Ferreira, M. A. (2020). Shear strength of prestressed 160 mm deep hollow core slabs. *Engineering Structures*, *218*, 110723. DOI: https://doi.org/10.1016/j.engstruct.2020.110723

Asamoto, S., Kato, K., & Maki, T. (2014). Effect of creep induction at an early age on subsequent prestress loss and structural response of prestressed concrete beam. *Construction and Building Materials*, *70*, 158-164. DOI: https://doi.org/10.1016/j.conbuildmat.2014.07.028

Associação Brasileira de Normas Técnicas [ABNT]. (2014). *Projeto de estruturas de concreto – Procedimento*. (NBR, 6118). Rio de Janeiro, RJ: ABNT.

Bastos, P. S. S. (2019a). *Fundamentos do concreto armado – notas de aula*. Bauru, SP: UNESP.

Bastos, P. S. S. (2019b). *Fundamentos do concreto protendido – notas de aula*. Bauru, SP: UNESP.

Biswal, S., & Ramaswamy, A. (2017). Uncertainty based model averaging for prediction of long-time prestress losses in concrete structures. *Construction and Building Materials*, *153*, 469-480. DOI: https://doi.org/10.1016/j.conbuildmat.2017.07.110

Breccolotti, M. (2018). On the evaluation of prestress loss in PRC beams by means of dynamic techniques. *International Journal of Concrete Structures and Materials*, *12*, 1-15. DOI: https://doi.org/10.1186/s40069-018-0237-8

Breccolotti, M. (2020). Eigenfrequencies of continuous prestressed concrete bridges subjected to prestress losses. *Structures*, *25*, 138-146. DOI: https://doi.org/10.1016/j.istruc.2020.03.011

Cao, Q., Tao, J., & Ma, Z. J. (2015). Prestress loss in externally FRP reinforced self prestressing concrete beams. *Construction and Building Materials*, *101*, 667-674. DOI: https://doi.org/10.1016/j.conbuildmat.2015.10.147

Caro, L. A., Martí-Vargas, J. R., Serna, P. (2013). Prestress losses evaluation in prestressed concrete prismatic specimens. *Engineering Structures*, *48*, 704-715. DOI: https://doi.org/10.1016/j.engstruct.2012.11.038

Carvalho, R. C. (2012). *Estruturas de concreto protendido: pós-tração; pré-tração; cálculo e detalhamento*. São Paulo, SP: PINI.

Cholfe, L., & Bonilha, L. A. S. (2018). *Concreto protendido: teoria e prática* (2nd ed.). São Paulo, SP: Oficina de Textos.

Dolan, C. W., & Hamilton, H. R. (2019). *Prestressed concrete: building, design, and construction*. Cham, Zug: Springer.

Guo, T., Chen, Z., Lu, S., & Yao, R. (2017). Monitoring and analysis of long-term prestress losses in post-tensioninged concrete beams. *Measurement*, *122*, 573-581. DOI: https://doi.org/10.1016/j.measurement.2017.07.057

Křístek, V., & Kadlec, L. (2017). Probabilistic analysis of prestress loss due to creep in concrete box girders. *Journal of Bridge Engineering*, *22*(12), 040171037. DOI: https://doi.org/10.1061/(asce)be.1943-5592.0001079

Marconato, L. S., & Sartorti, A. L. (2015). *Avaliação da perda de protensão por deformação da ancoragem na pós-tração através de método alternativo*. Engenheiro Coelho, SP: UNASP.

Michelini, E., Bernardi, P., Cerioni, R., & Belletti, B. (2020). Experimental and numerical assessment of flexural and shear behavior of precast prestressed deep hollow-core slabs. *International Journal of Concrete Structures and Materials*, *14*(31), 1-17. DOI: https://doi.org/10.1186/s40069-020-00407-y

Myers, J. J., & Bloch, K. E. (2013). Comparison of prestress losses for pedestrian bridges constructed with high-Strength concrete and high-strength self-consolidating concrete. *Journal of Bridge Engineering*, *18*(9), 871-878. DOI: https://doi.org/10.1061/(ASCE)BE.1943-5592.0000431

Naaman, A. E. (2012). *Prestressed concrete analysis and design: fundamentals* (3rd ed.). Ann Arbor, MI: Techno Press 3000.

Páez, P. M., & Sensale, B. (2018). Improved prediction of long-term prestress loss in unbonded prestressed concrete members. *Engineering Structures*, *174*, 111-125. DOI: https://doi.org/10.1016/j.engstruct.2018.07.038

Precast/Prestressed Concrete Institute [PCI]. (2017). *PCI Design Handbook: Precast and Prestressed Concrete* (8th ed.). Chicago, IL: PCI.

Sartorti, A. L. (2018). *Estruturas de concreto protendido – notas de Aula*. Engenheiro Coelho, SP: UNASP.

Shao, X., Pan, R., Zhao, H., & Shao, Z. (2014). Prestress loss of a new vertical prestressing anchorage system on concrete box-girder webs. *Journal of Bridge Engineering*, *19*(2), 210-219. DOI: https://doi.org/10.1061/(ASCE)BE.1943-5592.0000522

Singh, B. P., Yazdani, N., & Ramirez, G. (2013). Effect of a time dependent concrete modulus of elasticity on prestress losses in bridge girders. *International Journal of Concrete Structures and Materials*, *7*(3), 183-191. DOI: https://doi.org/10.1007/s40069-013-0037-0

Ward, D. B., Dang, C. N., Floyd, R. W., & Hale, W. M. (2016). Prestress losses of double-tee girders cast with lightweight self-consolidating concrete. *Journal of Building Engineering*, *7*, 133-142. DOI: https://doi.org/10.1016/j.jobe.2016.06.004

Xie, J., Cui, N., Yan, J., & Yu, J. (2019). Experimental study on prestress losses of post-tensioned concrete members at ultra-low temperatures. *Structural Concrete*, *20*(6), 1828-1841. DOI: https://doi.org/10.1002/suco.201800264

Yang, M., Gong, J., & Yang, X. (2020). Refined calculation of time-dependent prestress losses in prestressed concrete girders. *Structure and Infrastructure Engineering*, *16*(10), 1-17. DOI: https://doi.org/10.1080/15732479.2020.1712438

Ye, C., Butler, L. J., Elshafie, M. Z. E. B., & Middleton, C. R. (2020). Evaluating prestress losses in a prestressed concrete girder railway bridge using distributed and discrete fibre optic sensors. *Construction and Building Materials*, *247*, 118518. DOI: https://doi.org/10.1016/j.conbuildmat.2020.118518